ELSEVIER

Journal of Power Sources 58 (1996) 145–151

JOURNAL OF POWER SOURCES

A model lithium-ion system based on the insertion properties of the spinel phase $Li_xMn_2O_4$, $(0<x<2)$

M.Y. Saïdi *, R. Koksbang, J. Barker

Valence Technology, Inc., 301 Conestoga Way, Henderson NV 89015, USA

Received 19 October 1995; revised 10 January 1996

Abstract

A model lithium-ion system, based on the manganese oxide, $Li_xMn_2O_4$, has been used to study the reversibility of the lithium insertion processes in both the approximate 3 V and 4 V versus Li/Li^+ voltage ranges. For the 3 and 4 V ranges, symmetrical cells with the configuration: $Li_{1+x}Mn_2O_4$/electrolyte/$Li_{1-x}Mn_2O_4$ were investigated, while asymmetrical cells, $Li_xMn_2O_4$/electrolyte/$Li_{1-x}Mn_2O_4$, were used to investigate the electrochemical properties of the 4 V range only. The relatively large voltage hysteresis for the symmetrical cell was considered to be due to the concurrent cubic to tetragonal symmetry change occurring for the electrode cycling over the lower voltage range. Impedance measurements confirm that the $Li_{1+x}Mn_2O_4$ electrode appears to possess significantly inferior electrochemical properties to the electrode covering the higher voltage range. The 4 V range studied in the asymmetrical configuration showed excellent reversibility towards lithium insertion and extraction.

Keywords: Lithium-ion cells; Manganese oxide

1. Introduction

$Li_xMn_2O_4$ is a potential material for use in rechargeable lithium batteries, particularly as the high voltage cathode material in lithium-ion cells using carbon-based anodes. The material offers a relatively high specific capacity at a potential exceeding approximately 3.8 V versus Li/Li^+ [1–6]. The cycling of 1 Li per Mn_2O_4 unit corresponds to a theoretical specific capacity of 148 mAh/g. Generally this figure is only approached at low cycling rates [3]. At another voltage range around 3 V versus Li/Li^+, $Li_xMn_2O_4$ is able to reversibly intercalate an amount of lithium similar to that at the high voltage range. It is therefore possible to utilize symmetrical cells incorporating two $LiMn_2O_4$ electrodes as a model system for the lithium-ion-type battery technology [7]. One of the key advantages to be gained from studying this kind of model lithium-ion system is the possibility of conducting detailed measurements on an electrochemical system without interference from an electrode which is significantly different from the electrode of interest. Both the $Li_{1-x}Mn_2O_4$ and $Li_{1+x}Mn_2O_4$ intercalation systems are fairly well characterized, and the electrochemical properties of the two voltage ranges have been described previously [1–10]. For this particular symmetrical lithium-ion cell, the cell is charged when lithium ions are extracted from the electrode covering the 4 V versus Li/Li^+ voltage range, and inserted into the electrode covering the approximate 3 V versus Li/Li^+ voltage range. The converse reactions occur during cell discharge. The cell is expected to produce an average cell voltage of around 1 V under normal operating conditions.

Lithium-ion cells containing two identical electrodes have previously been used successfully, to characterize symmetrical cells based on amorphous V_2O_5 [11], V_6O_{13} [12], $LiTi_2O_4/LiNiO_2$ [13] as well as spinel-type compounds [7,14]. Here we will present data on two cell configurations, based on the $LiMn_2O_4$ spinel, used to investigate the electrochemical behavior of lithium insertion and extraction in the 3 and 4 V ranges.

2. Experimental

$LiMn_2O_4$ was prepared by firing appropriate amounts of MnO_2 and Li_2CO_3 to 800 °C for 48 h in open air. Powder X-ray diffraction (XRD) (Siemens D5000, Cu K_α radiation) was used to ascertain the phase purity of the compounds. No other crystalline phases were detected. Values of 8.227(2) Å for the unit cells parameters (*Fd3m* space group, $Z=8$), compare well with the literature data [1]. The average particle size of the $LiMn_2O_4$ material was about 6 μm as meas-

* Corresponding author.

PII S0378-7753(96)02383-1

ured using a Coulter Multisizer II. Lithium and manganese contents were determined from atomic absorption using an Instrumentation Laboratory AA/AE spectrophotometer model 357. For the asymmetrical cells:

$$Li_xMn_2O_4/electrolyte/Li_{1-x}Mn_2O_4 \quad (1)$$

one of the electrodes consisted of $LiMn_2O_4$ and the other of $LiMn_2O_4$ that has previously been electrochemically de-lithiated to $Li_xMn_2O_4$ at a very low current density (50 μA/cm^2). The cell balance was adjusted so that one of the electrodes was limiting. The symmetrical cells were constructed from two identical $LiMn_2O_4$ electrodes. The preparation of the polymeric electrolyte by radiation polymerization, which was used as both the electrode separator and as the binder in the composite cathode has been described elsewhere [15,16]. The electrolyte was prepared by electron beam curing of acrylate monomers, and the ionic conductivity was enhanced by plasticizing the polymer matrix with a 1 M $LiPF_6$/PC solution (77% by weight). The room temperature conductivity of the electrolyte exceeds 1 mS/cm, and the salt diffusion coefficient was measured to be in the range 10^{-6}–10^{-5} cm^2/s, i.e. the electrical properties are comparable with those of liquid organic electrolytes [17].

Three electrode cells using a lithium reference electrode were used for all measurements. The entire assembly was placed in a flexible encapsulation which was heat sealed under vacuum. The electrode geometric surface areas were typically 12 cm^2.

Voltage traces were recorded using the electrochemical voltage spectroscopy (EVS) technique originally devised by Thompson [18,19] to investigate lithium intercalation reactions in TiS_2, and later used to study similar reactions in conducting polymers [20], $Li_xMn_2O_4$ [2,3] and $LiCoO_2$ [21]. This technique yields information regarding structural phase changes and order/disorder phenomena [22,23]. The electrochemical measurements were conducted under thermostatic conditions at 23 °C, using either an Advantest R6142 precision voltage sink/source coupled to a HP Model HP3144A digital multimeter, or alternatively a Schlumberger Instruments model 1286 Electrochemical interface. Some of the more detailed electrochemical measurements were carried out using a recent adaptation of the EVS method developed for investigation of intercalation systems in which the electrochemical cell under test incorporates a suitable reference electrode [24,25]. For successful implementation of the so-called three-electrode EVS (TEVS) experiments, two additional high impedance followers are required. The technique allows determination of detailed information for both insertion electrodes simultaneously within a single experiment. It is thus well developed for investigation of lithium-ion-type battery systems [25].

Cells were also cycled galvanostatically at a current density of 0.2 mA/cm^2, in both charge and discharge, between preset voltage limits chosen to be symmetrical around 0 V and ranging from −1.0/+1.0 V to −2.5/+2.5 V for the symmetrical cells and −0.8/+0.8 V for the asymmetrical cells.

The a.c. impedance measurements were carried out on similar three-electrode cells to those described above using the Schlumberger Instruments model 1286 electrochemical interface coupled to a model 1255 frequency response analyzer. The measurements were conducted in the frequency range from 65 kHz to 1 Hz at an amplitude of ±10 mV.

3. Results and discussion

3.1. Electrochemical voltage spectroscopy data

The EVS and TEVS conditions chosen for cycling of the $Li_{1-x}Mn_2O_4/Li_{1+x}Mn_2O_4$ symmetrical cells included voltage limits between 0 and 1.6 V, voltage step sizes of 10 mV and critical current density I_{lim} < 50 μA/cm^2, equivalent to a charge/discharge rate of approximately $C/100$. These particular experimental conditions were chosen so as to maintain the system close to thermodynamic equilibrium throughout the discharge/charge cycle. As such, the voltage profile should provide a close approximation to the open-cell voltage (OCV)–charge capacity relationship for the cell. The EVS voltage profile for a typical cell is shown in Fig. 1(a), and

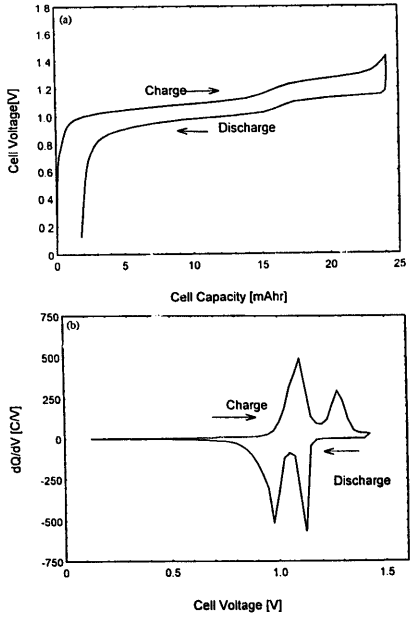

Fig. 1. (a) Total cell voltage of the second cycle of a representative $Li_{1-x}Mn_2O_4/Li_{1+x}Mn_2O_4$ cell obtained under EVS conditions. (b) Corresponding differential capacity plot.

the corresponding differential capacity in Fig. 1(b). The shape of the voltage curves indicate whether a region is single or multi-phase. In the latter case the potential is expected to be essentially invariant with composition. However, the distinction between single-phase behavior and multi-phase behavior is simplified when differential capacity curves are considered since composition independent behaviors appear as distinct differential capacity peaks. Furthermore, for highly reversible intercalation systems there should be insignificant displacement of the corresponding differential capacity feature during cathodic and anodic scans.

The variation of the cell potential for the complete cell, Fig. 1(a), indicates the presence of two plateaus during the lithium insertion/extraction processes. The two electrodes in the cell were selected so that they possess approximately equivalent lithium capacities. It is expected that slight capacity differences would result in a deviation from the predicted behavior. The major part of the measured curve, shows a single, rather flat plateau above 1 V together with another less well-defined plateau at about 1.25 V. The measured discharge capacity for the symmetrical cell corresponds to a material utilization figure of around 101 mAh/g for each of the $Li_xMn_2O_4$ electrodes (i.e. $x=0.68$, assuming that the cycling of $x=1$ in $Li_{1-x}Mn_2O_4$ or $Li_{1+x}Mn_2O_4$ corresponds to a specific capacity of 148 mAh/g). This is somewhat lower than the specific capacities measured during cycling of manganese oxide half-cells made from the same electrode stock and may indicate an imbalance in the two electrode specific capacities within the symmetrical cell. The observed hysteresis between the charge and discharge curves is indicative of the extent of the total overvoltage in the system.

Fig. 1(b) gives the corresponding and complementary differential capacity plot for the cell. It is demonstrated clearly that the cell voltage versus capacity plot is structured during the charge/discharge cycle shown in Fig. 1(a). There are two well-defined voltage regions for the lithium insertion/extraction reactions in the system as indicated by the distinct and reversible peaks shown in the figure. This behavior is consistent with the voltage data described in Fig. 1(a). The charge/discharge behavior appears to be relatively reversible (both coulombically and energetically) as indicated by the symmetrical nature of the anodic and cathodic waves. There is a significant level of overvoltage in the system as indicated by the degree of voltage hysteresis between equivalent anodic and cathodic peaks. There is no evidence consistent with electrolyte degradation as would be suggested by the presence of irreversible peaks.

The individual electrode potentials and the corresponding differential capacity curves are given for the 4 V and the 3 V voltage regions in Figs. 2 and 3, respectively, as determined by the TEVS technique. Fig. 2(a) shows the two distinct voltage plateaus observed in the 4 V region, as expected. The complementary differential capacity plot has two sharp peaks, with only minor overlap of the anodic and cathodic waves. This behavior is consistent with ordering of the inserted Li ions over the tetrahedral 8(a) sites that are occupied during

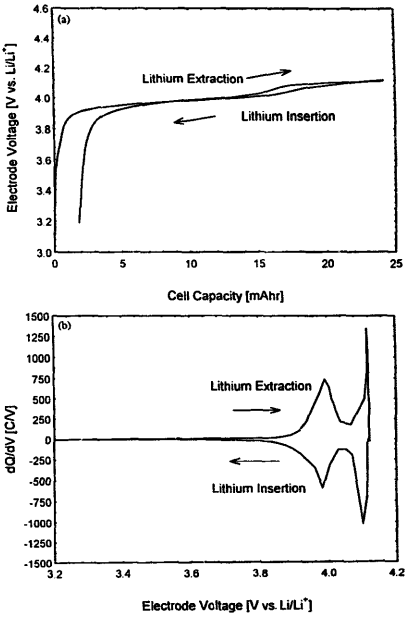

Fig. 2. (a) Approximate 4 V vs. Li/Li^+ voltage range trace for the second cycle of a representative $Li_{1-x}Mn_2O_4/Li_{1+x}Mn_2O_4$ cell obtained under TEVS conditions using an Li reference electrode. (b) Corresponding differential capacity plot.

the 4 V range. A small fraction of the capacity is lost during each cycle, again presumably due to capacity differences between the two electrodes. However, the reaction is highly reversible as indicated by the low overvoltage between the charge and discharge waves and the high coulombic reversibility of the reaction. Similar features are observed at the 3 V voltage range (Fig. 3), i.e. two plateaus, but the hysteresis between the charge and discharge curves is significantly more pronounced than at the 4 V voltage range. It is well known that at 3 V the lithium insertion in $Li_{1+x}Mn_2O_4$ electrode proceeds as a two phase reaction, in the complete range of x ($1<x<2$) [4], and should therefore yield a single plateau over this range. The presence of two plateaus is unclear but has been reported for lithium insertion in $LiMn_2O_4$ at 100 °C [26].

3.2. Impedance data

Fig. 4 shows the Nyquist a.c. impedance spectra for the two electrodes covering the approximate 3 V and 4 V versus Li/Li^+ voltage ranges. As denoted in the figure, the precise electrode potentials were 2.90 and 4.11 V versus Li/Li^+,

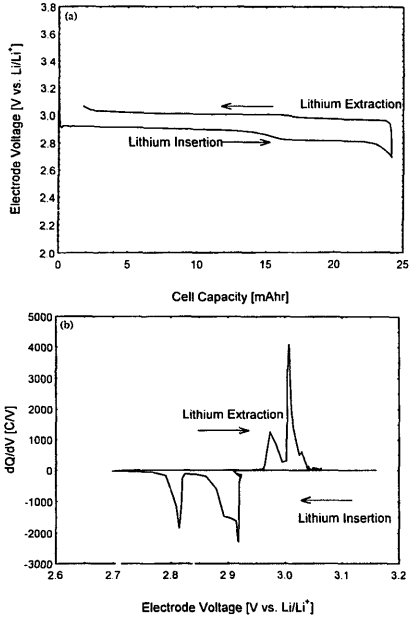

Fig. 3. (a) Approximate 3 V vs. Li/Li^+ voltage range trace for the second cycle of a representative $Li_{1-x}Mn_2O_4/Li_{1+x}Mn_2O_4$ cell obtained under TEVS conditions using an Li reference electrode. (b) Corresponding differential capacity plot.

respectively. Recall, these measurements were made on initially compositionally identical electrodes (via the lithium metal reference electrode) each of which had a geometric surface area of 12 cm^2. The lower voltage electrode generates a relatively high overall electrode impedance (serial resistance, $R_s = 0.51\ \Omega$ and charge-transfer resistance, $R_{ct} = 25\ \Omega$). The value of R_s is consistent with the expected high frequency impedance contributions from the electrolyte and the electrical contacts, etc. The charge-transfer impedance, however, is particularly large when compared to equivalent measurements on similarly formulated and comparably-sized composite intercalation electrodes [27]. This behavior is consistent with the characteristics of the EVS voltage traces shown in Fig. 3 (a) which show the presence of large voltage hysteresis (i.e. reaction overvoltage) between the cathodic (intercalation) and anodic (de-intercalation) waves. Thackeray et al. [28] have reported on the poor cycling of $Li/Li_xMn_2O_4$ cells over the 3 V voltage range and attributed this to an asymmetric lattice expansion/contraction of the $Li_xMn_2O_4$ electrode. They contested that the lattice disruption resulted from a Jahn–Teller distortion that occurs around $x = 1.08$ and which transforms the cubic symmetry of the

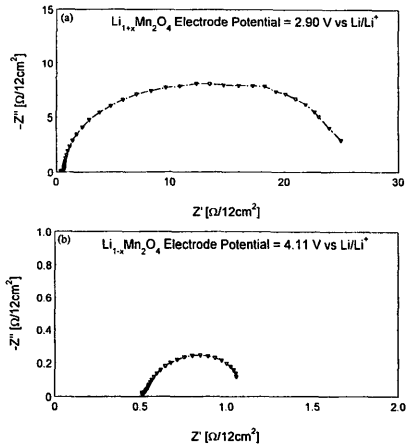

Fig. 4. (a) Nyquist a.c. impedance plot for the $Li_{1+x}Mn_2O_4$ electrode covering the approximate 3 V vs. Li/Li^+ voltage range. (b) Nyquist a.c. impedance plot for the $Li_{1-x}Mn_2O_4$ electrode covering the approximate 4 V vs. Li/Li^+ voltage range.

spinel phase to a tetragonal symmetry. Several attempts to stabilize the Jahn–Teller distortion have been reported (see for example Ref. [29]). We report our findings on the extended cycling properties of the $Li_{1+x}Mn_2O_4$ electrode in a future publication [30,31].

In direct contrast to the lower voltage electrode, the $Li_{1-x}Mn_2O_4$ electrode shows reasonably good impedance properties (i.e. $R_s = 0.51\ \Omega$ and $R_{ct} = 0.6\ \Omega$). These impedance properties are consistent with other well-formulated composite insertion-type electrodes such as the V_6O_{13} system [27,32]. The calculated R_s is consistent with the expected high frequency contributions to the system. The overall electrode impedance measured from the a.c. method is entirely consistent with the low overvoltage present in the EVS voltage traces described here (Fig. 4(b)) and also previously described by this group and others [2–6]. The retention of the cubic symmetry for the $Li_{1-x}Mn_2O_4$ electrode over this voltage range apparently produces a low interfacial charge-transfer impedance for the system. Again, in contrast to the lower voltage electrode, this confirms that the electrode is well suited for use in intercalation-type applications, such as the lithium-ion technologies. The low overvoltage (shown from the EVS data), and the relatively facile solid state diffusion [2] within the electrode produces an electrode with desirable rate capability. The cycling performance for the $Li_{1-x}Mn_2O_4$ electrode will be reported in a future publication [30]. Tarascon et al. [5,6,33,34] have previously demonstrated a reasonable cycle life coupled to a relatively low specific capacity fade for this material over a similar voltage range.

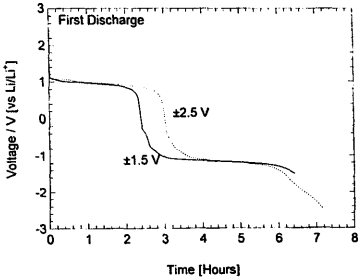

Fig. 5. Voltage traces of a representative $Li_{1-x}Mn_2O_4/Li_{1+x}Mn_2O_4$ cell cycled between voltage limits of −1.5 to +1.5 V and −2.5 to +2.5 V, respectively.

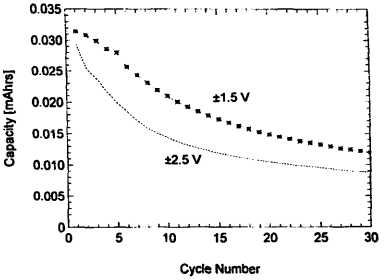

Fig. 6. Cycling curves of the $Li_{1-x}Mn_2O_4/Li_{1+x}Mn_2O_4$ cell cycled between voltage limits of −1.5 to +1.5 V and −2.5 to +2.5 V, respectively.

3.3. Cycling of symmetrical cells

Ideally, the voltage of an $Li_{1-x}Mn_2O_4/Li_{1+x}Mn_2O_4$ cell falls in the range 1−1.5 V. Typical voltage traces for cell cycling between −1.5 to +1.5 V and −2.5 to +2.5 V (at 0.2 mA/cm² in both charge and discharge) are compared in Fig. 5. The bi-polar nature of these cycling regimens means that each electrode will be cycling over both the 3 V and 4 V versus Li/Li^+ voltage ranges. Extension of the voltage limits to −2.5/+2.5 V, significantly increases the initial discharge capacity of the cell. However, as demonstrated by comparison of the cycling curves (Fig. 6), the discharge capacity decays more rapidly with cycle number in this case. Any additional discharge capacity for this increased voltage range is quickly lost from the system. After a few cycles the capacities of both cells are essentially identical. However, even when the voltage limits are reduced to −1.5/+1.5 V (and −1/+1 V, not shown), the discharge capacity steadily declines during cycling. Since both electrodes have identical loading, this supports the previously held assumption that the electrochemical properties of the lithium-insertion process into the $Li_{1+x}Mn_2O_4$ electrode (i.e. at voltages below 3 V versus Li/Li^+) are inferior to those for the higher voltage range.

3.4. Asymmetrical cell cycling data

The configuration of the asymmetrical cells, denoted as $Li_xMn_2O_4/Li_{1-x}Mn_2O_4$, was such that roughly one lithium per Mn_2O_4 unit would be shuttled back and forth into the system therefore looking exclusively at the 4 V response in both electrodes via the lithium reference electrode. Fig. 7 shows a typical voltage response for such a cell during the second cycle. The second cycle was chosen so as to minimize the small first cycle irreversible losses. The total cell voltage is shown in the lower half of the graph while the two upper curves represent the individual responses from the corresponding half-cells. As expected the responses are close mirror images of one another. While cathode '1' is being discharged, cathode '2' is being charged. At the cross point

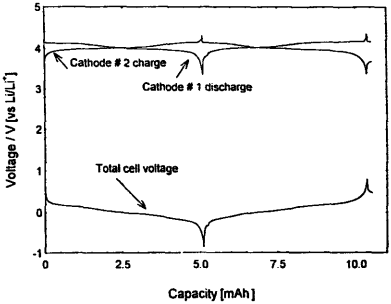

Fig. 7. Second cycle voltage trace of a three-electrode $Li_xMn_2O_4/Li_{1-x}Mn_2O_4$ asymmetrical cell.

between the two upper curves, the relative amounts of lithium in both electrodes should be the same. Therefore, the measured voltage across the cell should be zero. The total cell response shows that this cross point occurs at a cell capacity of ≈2.5 mAh corresponding to a material utilization of 68 mAh/g or $x \approx 0.46$ Li in both electrodes. This value is higher than that reported for $LiMn_2O_4$ when cycled against a lithium electrode (under the same cycling conditions). Therefore, one is looking at the intrinsic properties of the spinel-based electrode without interferences from either a lithium or a carbon electrode.

To gain a clearer insight into the electrochemical capabilities of the $LiMn_2O_4$ based electrode, asymmetrical cells were cycled at a current density of 0.25 mA/cm² in both charge and discharge between voltage limits of −0.8 and +0.8 V. After 500 cycles, the cell was suspended at which point a differential capacity measurement carried under EVS conditions was performed. We specifically chose this technique as a tool to probe any changes the electrodes had undergone. Any structural or electrochemical irreversibility associated with electrode degradation should be seen clearly in the differential capacity curves. Fig. 8 shows a differential capacity trace for a fresh cell (only one half of the cell is shown) and

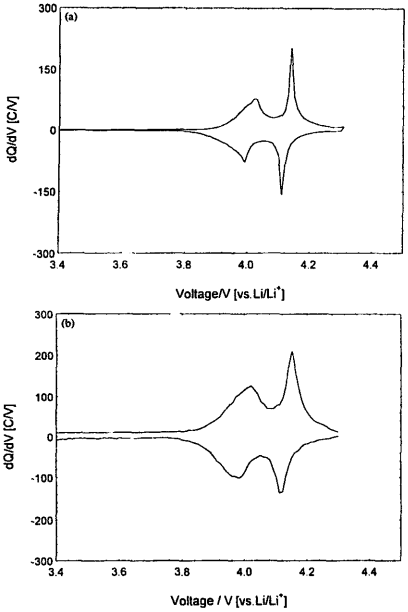

Fig. 8. (a) Differential capacity curve of an $LiMn_2O_4$-based electrode (second cycle). (b) Differential capacity curve of an $LiMn_2O_4$-based electrode after 500 cycles.

compared with the same cell that had undergone 500 cycles. Fig. 8(a) is a typical differential capacity plot for an optimized $LiMn_2O_4$ based electrode. The traces are similar, apart from a slight broadening of the relative peaks (corresponding to plateaus in the voltage–composition curve) and a lower capacity associated with the cycled cell which is to be expected. Overall, this finding highlights the high reversibility of lithium insertion/extraction in this system.

Extended cycling of a typical asymmetrical cell is presented in Fig. 9. Similarly to the voltage profile trace (Fig. 7), both the discharge and charge capacities variation with cycle number are presented. Over a 1000 cycles have been achieved with this type of cell configuration. The specific capacity of the $Li_{1-x}Mn_2O_4$ at this stage was still a very respectable 75 mAh/g.

4. Conclusions

The voltage hysteresis, i.e. the reaction overvoltage, between the cathodic and anodic waves present during cycling of the $Li_{1-x}Mn_2O_4/Li_{1+x}Mn_2O_4$ cell was predicted from the half-cell responses and is expected to be mainly due to intercalation properties of the electrode covering the approximate 3 V versus Li/Li^+ voltage range. The relatively large overvoltage for this voltage range was considered to be due to the structural changes occurring within this electrode material during lithium insertion/extraction reactions. The lattice disruption results from a Jahn–Teller distortion that occurs around $x = 1.08$ and which transforms the cubic symmetry of the spinel phase to a tetragonal symmetry [28]. Conversely, the $Li_{1-x}Mn_2O_4$ electrode (covering the approximate 4 V versus Li/Li^+ voltage range) showed extremely low overvoltage consistent with previously reported data from this group and elsewhere [2–6]. Over this voltage range the cubic symmetry of the spinel phase is retained during the insertion/extraction reactions.

Low rate cycling (TEVS) of cells utilizing a lithium metal reference electrode indicated that the $Li_{1-x}Mn_2O_4/Li_{1+x}Mn_2O_4$ cell demonstrates a discharge capacity which corresponds to a material utilization figure of around 101 mAh/g for each of the manganese oxide electrodes (i.e. $x = 0.68$, assuming the cycling of $x = 1$ in $Li_{1-x}Mn_2O_4$ or $Li_{1+x}Mn_2O_4$ corresponds to a specific capacity of 148 mAh/g).

Representative $Li_{1-x}Mn_2O_4/Li_{1+x}Mn_2O_4$ cells were cycled between pre-set voltage limits of -1.5 to $+1.5$ V and -2.5 to $+2.5$ V at a current density of 0.2 mA/cm^2 in both charge and discharge. The bi-polar nature of these cycling

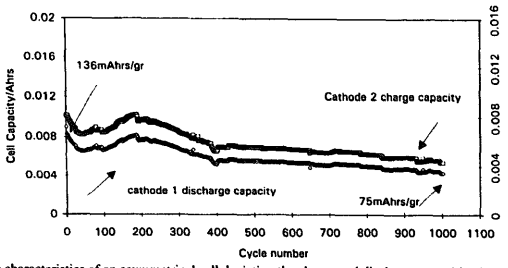

Fig. 9. Extended cycling characteristics of an asymmetrical cell depicting the charge and discharge capacities for both individual electrodes.

regimens means that each electrode would be cycled over both the approximate 3 V and 4 V versus Li/Li^+ voltage ranges during the normal discharge/charge cycles of these cells. After a few cycles the capacity of both cells were essentially identical. Over extended cycling periods, the cells, regardless of cycling voltage limits, exhibited declining discharge capacities. We believe this phenomenon is due to the poor cycling capability of the electrode over the 3 V versus Li/Li^+ voltage range, induced primarily by the afore-mentioned structural phase transition, caused during the lithium insertion/extraction reactions.

The a.c. impedance measurements also indicated that the interfacial properties for the electrode covering the upper voltage range are far superior to those for the lower voltage range. This is consistent with the pronounced overvoltage present on the TEVS measurements for the 3 V versus Li/Li^+ and again, is presumably directly related to the cubic to tetragonal symmetry change.

The asymmetrical cells ($Li_xMn_2O_4$/electrolyte/$Li_{1-x}Mn_2O_4$) provided a good vehicle for the investigation of the electrochemical properties in the 4 V range. Excellent reversibility was demonstrated. Under the cycling conditions used in this work, over a 1000 cycles have been achieved with only minor degradation to the electrode.

References

[1] A. Mosbah, A. Verbaere and M. Tournoux, *Mater. Res. Bull.*, *18* (1983) 1375.

[2] J. Barker, R. Pynenburg and R. Koksbang, *J. Power Sources*, *52* (1994) 185.

[3] J. Barker, K. West, Y. Saidi, R. Pynenburg, B. Zachau-Christiansen, I.I. Olsen and R. Koksbang, *J. Power Sources*, *54* (1995) 475.

[4] M.M. Thackeray, *Prog. Batteries Battery Mater.*, *14* (1995) 1173.

[5] F.K. Shokoohi, J.M. Tarascon and D. Guyomard, *Prog. Batteries Battery Mater.*, *14* (1995) 173.

[6] F.K. Shokoohi, J.M. Tarascon and D. Guyomard, *Prog. Batteries Battery Mater.*, *14* (1995) 199.

[7] M.M. Thackeray, P.J. Johnson, L.A. de Picciotto, P.G. Bruce and J.B. Goodenough, *Mater. Res. Bull.*, *19* 179 (1984).

[8] M.M. Thackeray, W.I.F. David, P.G. Bruce and J.B. Goodenough, *Mater. Res. Bull.*, *18* 461 (1983).

[9] J.C. Hunter, *J. Solid State Chem.*, *39* (1981) 142.

[10] T. Ohzuku, M. Kitagawa and T. Hirai, *J. Electrochem. Soc.*, *137* (1990) 769.

[11] T. Shodai, Y. Sakurai, S. Okada, Y. Nemoto and J. Yamaki, *Ext. Abstr., The Electrochemical Society Fall Meet., Miami, FL, USA, 9–14 Oct. 1994*, Vol. 94–2, The Electrochemical Society, Pennington, NJ, USA, Abstr. No. 98, pp. 156.

[12] R. Koksbang, J. Barker and Y. Saidi, *Prog. Batteries Battery Mater.*, *14* (1995) 125.

[13] T. Ohzuku, A. Ueda, N. Yamamoto and Y. Iwakoshi, *J. Power Sources*, *54* (1995) 99.

[14] E. Ferg, R. J. Gummow, A. de Kock and M.M. Thackeray, *J. Electrochem. Soc.*, *141* (1994) L147.

[15] R. Koksbang, F. Flemming, I.I. Olsen, P.E. Tønder, K. Brøndum, M. Consigny, K.P. Petersen and S. Yde-Andersen, in K.M. Abraham and M. Solomon (eds.), *Proc. Symp. Primary and Secondary Lithium Batteries*, Proc. Vol. 91–3, The Electrochemical Society, Pennington, NJ, USA, 1991, pp. 157.

[16] I.I. Olsen, *Ph.D. Thesis*, University of Odense, Denmark, 1994.

[17] H.V. Venkatasetty (ed.), *Lithium Battery Technology*, Wiley, New York, 1984, p. 39.

[18] A.H. Thompson, *Phys. Rev. Lett.*, *23* (1978) 1511.

[19] A.H. Thompson, *J. Electrochem. Soc.*, *126* (1979) 608.

[20] J. Barker, *Synth. Met.*, *32* (1989) 43.

[21] R. Pynenburg, J. Barker, R. Koksbang and Y. Saïdi, *Ext. Abstr., The 185th Electrochemical Society Spring Meet.*, Vol. 94–1, The Electrochemical Society, Pennington, NJ, USA, Abstr. No. 578, p. 923.

[22] T. Jacobsen, K. West and S. Atlung, *Electrochim. Acta*, *27* (1982) 1007.

[23] O. Tillement and M. Quarton, *J. Electrochem. Soc.*, *140* (1993) 1870.

[24] J. Barker, D. Baldwin, D.C. Bott and S.J. Porter, *Synth. Met.*, *28* (1989) D127.

[25] J. Barker, *Electrochim. Acta*, *40* (1995) 1603.

[26] R. Koksbang, J. Barker, M.Y. Saïdi, K. West, B. Zachau-Christiansen and S. Skaarup, *Solid State Ionics*, *83* (1996) 35.

[27] J. Barker and R. Koksbang, *Electrochim. Acta*, *40* (1995) 673.

[28] M.M. Thackeray, A. de Kock, M.H. Rossouw, D. Liles, R. Bittihn and D. Hoge, *J. Electrochem. Soc.*, *139* (1992) 363.

[29] H. Huang and P. G. Bruce, *J. Electrochem. Soc.*, *141* (1994) L76.

[30] M.Y. Saïdi, J. Barker and R. Koksbang, *Electrochim. Acta*, in preparation.

[31] M.Y. Saïdi, R. Koksbang, H. Shi and J. Barker, *IBA Meet., 7–8 Oct. 1995, Chicago, IL, USA.*

[32] R Koksbang, I.I. Olsen, P.E. Tønder, N. Knudsen and D. Fauteux, *J. Appl. Electrochem.*, *21* (1991) 301.

[33] J.M. Tarascon, D. Guyomard and G.L. Baker, *J. Power Sources*, *43/44* (1993) 293.

[34] J. M. Tarascon and D. Guyomard, *Solid State Ionics*, *69* (1994) 293.